Combined omics approaches reveal distinct responses between light and heavy rare earth elements in *Saccharomyces cerevisiae*

Nicolas Grosjean[1,2,†], Marie Le Jean[2], Jean Armengaud[3], Adam Schikora[4], Michel Chalot[5,6], Elisabeth M. Gross[2], Damien Blaudez[1]*

[1]*Université de Lorraine, CNRS, LIEC, F-54000 Nancy, France*
[2]*Université de Lorraine, CNRS, LIEC, F-57000 Metz, France*
[3]*Université Paris-Saclay, CEA, INRAE, Département Médicaments et Technologies pour la Santé (DMTS), SPI, 30200 Bagnols-sur-Cèze, France*
[4]*Institute for Epidemiology and Pathogen Diagnostics, Julius Kühn Institute (JKI) - Federal Research Centre for Cultivated Plants, 38104 Braunschweig, Germany*
[5]*Université de Bourgogne Franche-Comté, CNRS, Laboratoire Chrono-Environnement, F-25000 Besançon, France.*
[6]*Université de Lorraine, F-54000 Nancy, France*
†Current affiliation; Biology Department, Brookhaven National Laboratory, Upton, NY 11973, USA

*Corresponding author:

Dr Damien Blaudez

UMR 7360 LIEC, Faculté des Sciences et Technologies

Université de Lorraine, BP70239

Vandoeuvre-lès-Nancy F-54506, France

Tel: +33-3-72-74-51-67

E-mail: damien.blaudez@univ-lorraine.fr

Highlights

- First proteo-transcriptomics analysis revealing yeast molecular response to REEs
- Rare earth elements trigger specific responses
- Yeast cells react differentially to light vs heavy REEs
- Cell wall organization and pheromone signalling pathways are key yeast responses

Keywords

Lanthanides; REEs; lanthanum; ytterbium; proteomics; transcriptomics; cell wall

Abstract

The rapid development of green energy sources and new medical technologies contributes to the increased exploitation of rare earth elements (REEs). They can be subdivided into light (LREEs)

and heavy (HREEs) REEs. Mining, industrial processing, and end-use practices of REEs has led to elevated environmental concentrations and raises concerns about their toxicity to organisms and their impact on ecosystems. REE toxicity has been reported, but its precise underlying molecular effects have not been well described. Here, transcriptomic and proteomic approaches were combined to decipher the molecular responses of the model organism *Saccharomyces cerevisiae* to La (LREE) and Yb (HREE). Differences were observed between the early and late responses to La and Yb. Several crucial pathways were modulated in response to both REEs, such as oxidative-reduction processes, DNA replication, and carbohydrate metabolism. REE-specific responses involving the cell wall and pheromone signalling pathways were identified, and these responses have not been reported for other metals. REE exposure also modified the expression and abundance of several ion transport systems, with strong discrepancies between La and Yb. These findings are valuable for prioritizing key genes and proteins involved in La and Yb detoxification mechanisms that deserve further characterization to better understand REE environmental and human health toxicity.

1. Introduction

The rare earth element (REE) metal group consists of yttrium (Y), scandium (Sc), and 15 lanthanides, spanning from lanthanum (La) to lutetium (Lu). REEs can be divided into two different groups known as light REEs (LREEs), which gather La, Ce, Pr, Nd, Pm, Sm, and Eu, and heavy REEs (HREEs), which include Gd, Tb, Dy, Y, Ho, Er, Tm, Yb, and Lu (Cotton, 2006). These elements display unique physical (magnetic) and chemical (catalytic) characteristics that make them essential for advanced technologies (e.g., green energy production, communication, screens, medicines, catalysts) (Ciacci et al., 2015). REEs are also used as fertilizers and food supplements for cattle, pigs, and chickens (He et al., 2001; He and Rambeck, 2000; Hu et al., 2004; Panichev, 2015). The expanding exploitation of REEs owing to their increased use and low recyclability (Binnemans et al., 2013; Ciacci et al., 2015) has generated concern regarding their subsequent environmental and toxicological impacts. High REE concentrations are found in the vicinity of REE mining sites and impact the surrounding environment, as well as human health (Lee and Wen, 2018; Noack et al., 2014; Wei et al., 2013). In this context, REEs have been categorized as emerging contaminants (Gwenzi et al., 2018; Souza et al., 2021).

REEs were initially considered harmless and nonessential elements (Leeuw and Academic, 2000; Setua et al., 2010). However, several recent studies demonstrated the ecotoxicological effect of such elements on both aquatic and terrestrial organisms, including mammals (Gonzalez et al., 2014; Pagano et al., 2015; Rim et al., 2013). REEs have been shown to display antibacterial, antifungal and nematicidal activities (Wakabayashi et al., 2016). They also affect urchin embryogenesis (Pagano et al., 2016; Trifuoggi et al., 2017) and human health (Pagano et al., 2015; Wei et al., 2013). More specifically, it was shown that REEs induced oxidative stress through the production of reactive oxygen species, lipid peroxidation, and the modulation of superoxide dismutase, catalase, and glutathione peroxidase in plants, fish, rats and mice and in animal cell lines (including human cells) (Babula et al., 2015; Gonzalez et al., 2014; Liang and Wang, 2013; Pagano et al., 2015; Xu et al., 2016). Other effects have been observed, such as membrane permeability alterations (El-Ramady, 2008; Gao et al., 2017; Técher et al., 2020; Weiwei et al., 2007; Yufeng et al., 2007), mitotic and chromosomal aberrations (Pagano et al., 2015), and the overproduction of exopolysaccharides (Fitriyanto et al., 2011) in microorganisms. However, these aspects of REE toxicity were investigated in diverse organisms, making it difficult to draw comprehensive

conclusions. Moreover, the precise underlying molecular mechanisms are not well described, and only a few studies have hypothesized that LREEs and HREEs might induce different cellular responses as a result of lanthanide contraction (a decreasing ionic radius with an increasing atomic mass) or due to their reactivity and chemical differences (Gonzalez et al., 2014; Wang et al., 2017). For instance, plants that accumulate REEs display specific enrichment of either LREEs or HREEs (Grosjean et al., 2020, 2019). Taken together, these few available studies support the need to elucidate the cellular and molecular mechanisms involved in the response to REEs, similar to work performed on the specific REE yttrium (Grosjean et al., 2018).

To decipher the cellular response to new stressors and pollutants such as REEs, combining different and complementary "omics" analyses can offer many benefits (Taymaz-Nikerel et al., 2016). There is a considerable amount of data regarding the exposure of yeast cells to various toxic metals (Wysocki and Tamás, 2010), and large-scale omics methods are powerful approaches for investigating metal stress in yeast (Hosiner et al., 2014; Jin et al., 2008; Taymaz-Nikerel et al., 2016). Such analyses with model organisms are especially relevant as a first step to better comprehend the functions involved in areas that have received little research attention. In our study, we investigated the unicellular eukaryotic model *Saccharomyces cerevisiae*, which has been remarkably informative and extensively used as a proxy for unravelling eukaryotic cellular machinery and mechanisms (Botstein et al., 1997; Kachroo et al., 2017). We hypothesized that REEs would impact the yeast physiology and that LREEs and HREEs would trigger different responses. To test our hypotheses, we chose La and Yb as a representative LREE and HREE, respectively. La was selected as it is the first element of the lanthanide series while Yb is almost the last and La and Yb are among the most extracted and the least recycled LREEs and HREEs, respectively (Ciacci et al., 2015). Additionally, we investigated whether REE-triggered responses would be the same as for other well-known toxic metals.

This is the first study that combines an investigation of the transcriptome and proteome of *S. cerevisiae* upon exposure to REEs. The transcriptional patterns were compared at two different effective concentrations of two REEs, and time-dependent proteomic profiles were obtained to provide the first insights into REE toxicity in this important eukaryotic model.

2. Materials and methods

2.1. Yeast strain, chemicals and REE toxicity tests

The wild-type strain BY4741 of *S. cerevisiae* (MATa; his3Δ1; leu2Δ0; met15Δ0; ura3Δ0) was used. REEs in their trichloride form were purchased from Sigma-Aldrich (MO, USA). To determine the EC_{10} (the concentration at which 10% of the population is inhibited) and EC_{50} (the concentration at which half of the population is inhibited), log-phase cells (OD_{600nm} 0.15) were exposed to increasing REE concentrations in modified YNB-β-glycerophosphate liquid medium (YNB medium lacking KH_2PO_4, substituted by 1 mM β-glycerophosphate to avoid REE precipitation, pH 5.8), and growth (OD_{600nm}) was recorded for 10 h at 28°C under constant shaking (180 rpm). The growth ratio (OD at 9 h over OD at 4 h) was measured in log-phase and plotted against the REE concentrations.

2.2. Sample preparation for RNA-seq analysis

The wild-type strain was grown in YNB-β-glycerophosphate liquid medium. Cultures were inoculated at an OD_{600nm} of 0.05, and once the cultures reached an OD_{600nm} of 0.6, the cells were exposed for 1 h to 50 or 160 µM lanthanum or to 6 or 8 µM ytterbium, corresponding to their EC_{10} and EC_{50}, respectively. The cells were then harvested by centrifugation at 4000 rpm for 1 min at room temperature and flash frozen. After cell disruption by bead beating, total RNA was column-

purified using an RNeasy mini kit (Qiagen, Les Ulis, France) according to the manufacturer's instructions, and the gDNA was removed using DNAse I (Sigma Aldrich). RNA integrity was further assessed using a Bioanalyzer 2100 (Agilent, CA, USA). Strand-specific cDNA libraries were prepared by Eurofins Genomics (Ebersberg, Germany) using the TruSeq-3 library kit. Sequencing was carried out on an Illumina HiSeq 2500 with chemistry v4 applying the high-output run mode and using 2x100 bp paired-end sequencing.

2.3. Analysis of differentially expressed (DE) genes

The data obtained were analysed using the online platform Galaxy (https://usegalaxy.org/). The reads were first trimmed using the Trimmomatic v0.36.1 tool to remove any remaining Illumina adaptor sequences and low-quality reads, and FastQC v0.67 was used to check read quality before and after the Trimmomatic step. Sorted trimmed reads were mapped to the reference genome (S288C R64-2-1 of 2015-01-31 from https://www.yeastgenome.org/) of *S. cerevisiae* using TopHat v2.1.1. Reads that were mapped to the reference genome were quantified using HTSeq-count v0.6.1p1. Finally, differential gene expression analysis between treatments was carried out using DESeq2 v1.14.1. Genes that were differentially expressed among the conditions were identified and expressed as the $\log_2$-fold change, with adjusted p-values calculated via the Benjamini-Hochberg test. A cut-off-adjusted p-value of < 0.01 was applied.

2.4. Sample preparation for proteomics analysis

The wild-type strain was grown as mentioned in section 2.1. Cultures were inoculated at an OD_{600nm} of 0.05. Once the cultures reached an OD_{600nm} of 0.6, the REEs were added at the EC_{50} concentration and exposed for 1 or 4 h. The cells were harvested by centrifugation at 4000 rpm at room temperature for 1 min. The cell pellets were washed twice with 50 mM PBS pH 7 and flash frozen. Proteins were extracted from the frozen cells by bead beating with a Precellys 24 instrument (Bertin) after the addition of 1X LDS (Invitrogen) consisting of 106 mM Tris-HCl, 141 mM Tris base, 2% (m/v) lithium dodecyl sulfate, 10% (m/v) glycerol, 0.51 mM EDTA, 0.22 mM SERVA Blue G250, 0.175 mM phenol red, buffered at pH 8.5 and supplemented with 2.5% (v/v) ß-mercaptoethanol. The samples were heated for 5 min at 95°C, loaded (25 µL per well) onto a 4-12% gradient 10-well NuPAGE denaturing gel (Invitrogen), and subjected to electrophoresis for 5 min as previously recommended (Hartmann et al., 2014). After rapid staining with Coomassie Blue Safe (Invitrogen), polyacrylamide bands corresponding to the whole proteomes were cut out of the gel, destained in ultrapure water, reduced with dithiothreitol, and treated with iodoacetamide before performing proteolysis with Trypsin Gold Mass Spectrometry Grade protease (Promega) in the presence of 0.01% (v/v) ProteaseMAX surfactant (Promega).

2.5. Tandem mass spectrometry

Tryptic peptides were subjected to tandem mass spectrometry with a Q-Exactive HF tandem mass spectrometer (Thermo Fisher Scientific, Les Ulis, France) incorporating an ultrahigh field Orbitrap analyser coupled in line to an Ultimate 3000 chromatography system (Thermo Fisher Scientific). The tandem mass spectrometer was operated in the data-dependent acquisition mode as previously described (Klein et al., 2016). Briefly, each sample (4 µL) was injected and desalted on a reverse-phase capillary C18 PepMap™ 100 precolumn (LC-Packing) and then peptides were resolved based on their hydrophobicity on a nanoscale 500-mm C18 PepMap 100 column (5 mm x 300 µm i.d., Thermo Fisher Scientific) using a 90-min gradient from 2.5% to 40% of 80% CH_3CN, 19.9% H_2O, and 0.1% formic acid. Once separated, mass spectra of the peptides were acquired in the full-scan range of 350-1800 *m/z* at a resolution of 60,000 and an AGC target of 3.10^6. Peptide ions with

charges of $^{2+}$ or $^{3+}$ were selected for fragmentation according to a Top20 method consisting of the sequential analysis of each of the 20 most abundant peptide ions. MS/MS mass spectra were acquired with an AGC target set at 10^4, a loop count of 60 ms, an isolation window of 1.6 *m/z*, a resolution of 15,000, a dynamic exclusion of 20 s, and a scan performed over a dynamic mass range from the first mass detected up to 15 times the first mass.

2.6. Peptide-to-spectrum assignment and protein identification

Peak lists were automatically generated from raw files with an in-house script using the Proteome Discoverer 1.4.1 (Thermo Fisher Scientific) daemon conversion function and the following options: minimum mass (400), maximum mass (5,000), grouping tolerance (0), intermediate scans (0), and threshold (1,000). MS/MS spectra from the resulting *.mgf files were assigned to *S. cerevisiae* peptide sequences with Mascot v2.5.1 (Matrix Science) with the following parameters: full trypsin specificity with up to two missed cleavages allowed, static modification of carbamidomethylated cysteine, variable deamidation of asparagine and glutamine, variable oxidation of methionine, mass tolerance of 5 ppm on parent ions and mass tolerance on MS/MS of 0.02 Da. Peptide matches with a Mascot peptide score below a p-value of 0.05 were parsed with IRMA (Dupierris et al., 2009). Proteins were validated when at least two different peptides were detected. The false discovery rate for protein identification was less than 1%, as estimated with the reverse database decoy Mascot search option. Spectral counts corresponding to the number of MS/MS spectra assigned per protein were extracted for each sample without applying the parsimony rule to avoid isoform quantitation bias. The normalized spectral abundance factor (NSAF) for each protein was calculated as the total spectral count divided by its molecular mass in kDa and presented as a percentage. Spectral counts were compared between conditions using the T-Fold method in PatternLab (Carvalho et al., 2012) after normalizing the spectral counts. The statistical classes were defined as "Blue" for proteins that satisfied both |T-fold| (≥ 1.5) and its associated p-value (≤ 0.05), "Orange" for proteins with identifications that did not meet the T-fold criterion (but should be further investigated because they had low p-values), "Green" for proteins that satisfied the fold criteria but were likely false positives, and "Red" for proteins that did not meet both fold and p-value criteria.

2.7. GO term enrichment analysis

Overrepresented gene ontology (GO) terms among differentially expressed genes (DEGs) and proteins (DEPs) in each condition tested were obtained using the online Database for Annotation, Visualization and Integrated Discovery (DAVID) tool (Huang et al., 2009a, 2009b). GO terms significantly overrepresented for biological pathways, cellular compartment, and molecular functions were selected with a set p-value cut-off of < 0.05. Kyoto Encyclopaedia of Genes and Genomes (KEGG) analysis was also performed on DEGs and DEPs using the online DAVID tool with the same cut-off. DEG and DEP heatmaps were obtained using the R package pheatmap v1.0.10 with a complete clustering method. Euclidian clustering distance measurement was selected for rows and columns. Venn diagrams were drawn using the R package Venneuler v1.1-0.

2.8. Elemental analyses

Yeast cultures were grown in YNB-β-glycerophosphate as previously mentioned. The cultures were inoculated at an OD_{600nm} of 0.05, and once the cultures reached an OD_{600nm} of 0.6, lanthanum and ytterbium were added at 50 µM and 6 µM, respectively. After 1 h of exposure to the REEs, the yeast cells were harvested by centrifuging at 4000 rpm for 1 min at 4°C. The cell pellets were

washed three times with ice-cold MES (20 mM) – EDTA (10 mM) buffer (pH 6), three times with ice-cold ultrapure water, and then dried for 48 h at 70°C. Triplicate samples were prepared. Aliquots (125 mg) were mineralized with 1.75 mL of ultratrace HNO_3 and 0.5 mL of ultratrace hydrogen peroxide in closed tubes placed in a block digestion system (DigiPREP, SCP Sciences, Courtaboeuf, France). Gradual heating was used to achieve a final temperature of 100°C (total heating time of 265 min). Ultrapure water was then added to a final volume of 12.5 mL. Blank and reference materials were digested under the same conditions as the samples. Concentrations of Mn, Mo and Zn were determined using inductively coupled plasma mass spectrometry (ICP-MS, X Series II Model, Thermo Fischer Scientific, Courtaboeuf, France). Other elements were analysed by inductively coupled plasma atomic emission spectroscopy (ICP-AES, Radial ICAP6500 Model, Thermo Fischer Scientific). The validity of the analytical methods was checked using certified reference material (oriental basma tobacco leaves, INCT-OBTL-5, LGC Promochem, Molsheim, France) (Table S1).

2.9. Data availability

The mass spectrometry and proteomics datasets are available through the ProteomeXchange Consortium via the PRIDE partner repository (https://www.ebi.ac.uk/pride/) under the dataset identifier PXD010700 and project DOI 10.6019/PXD010700. The RNA-seq datasets are available in the NCBI GEO repository (GSE175826).

3. Results and discussion

3.1. REE toxicity assessment

To compare the cellular toxicity of La and Yb, the yeast EC_{10} and EC_{50} were first established for the two elements. For this, *S. cerevisiae* was exposed to increasing concentrations of these two REEs, and the cellular density was monitored every hour for nine hours (Fig. 1a,c). Different concentration ranges were used for La and Yb because preliminary tests showed a higher toxicity of Yb than La (data not shown). The growth ratio between 9 and 4 hours was then plotted against the REE concentration to determine the EC_{10} and EC_{50} values (Fig. 1b,d). Yb was 20 times more toxic than La, which is in line with observations using *Escherichia coli* (Técher et al., 2020). The respective EC_{10} and EC_{50} values for La were calculated to be 50 µM and 160 µM and were 6 µM and 8 µM for Yb (Fig. 1b,d).

We also investigated the effect of La and Yb exposure on the elemental composition of the cells (Fig. 1e). We observed an increase in the Mn (18 to 50%), Fe (29 to 42%), Zn (13 to 18%) and Cu (80 to 84%) concentrations under both La and Yb exposures. Under Yb exposure, the Ca (10-fold) and Na (4-fold) concentrations increased, whereas their concentrations were less affected by exposure to La (2-fold increase for Ca at La EC_{10}). The only decreased elemental concentration observed was for K (-20%) under Yb exposure (Fig. 1e). The decrease in K was probably triggered to counterbalance the increase in Ca and Na to maintain the cationic balance in the cells. Another hypothesis is that REEs can induce plasma membrane permeabilization as observed in other organisms (Ramos et al., 2016; Técher et al., 2020). Permeabilization of the plasma membrane would allow the nonspecific influx of ions in the cells, explaining the observed increase of cellular cation content following La and Yb exposure. In addition to these preliminary investigations of REE-dependent ionome alterations and La- and Yb-triggered toxicity, the EC_{10} and EC_{50} were chosen to further study the common and potentially specific yeast cell responses to these different lanthanides through transcriptomic and proteomic analyses (Fig. 1f).

Prior to describing the cellular mechanisms involved in the response to the different REEs, we first compared the transcriptome of yeasts exposed to the EC_{10} and EC_{50} of the two REEs to test whether different responses would be observed at these two concentrations. The time-evolving proteome was also monitored and analysed.

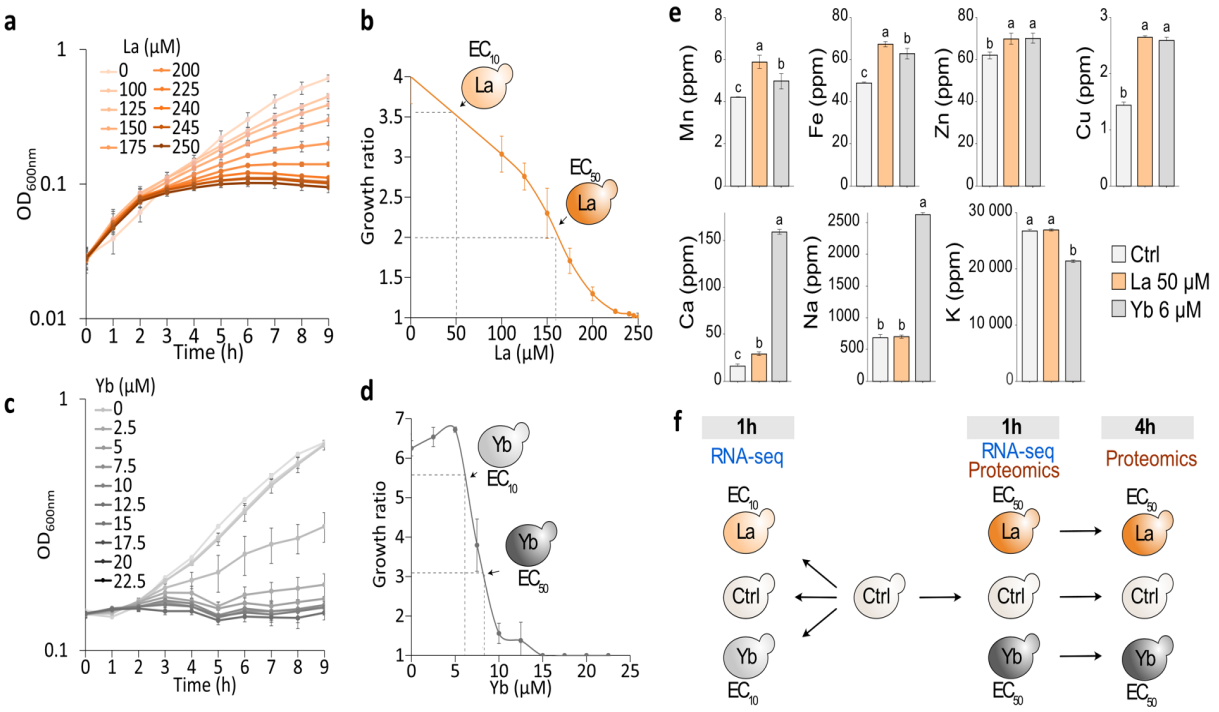

Figure 1. Impact of REEs on *Saccharomyces cerevisiae* growth and ionome and the omics experimental setup approach. (a) Growth of yeast exposed to different La concentrations. (b) Growth ratio (OD at 9 h over OD at 4 h) of yeast exposed to increasing amounts of La, enabling the identification of the EC_{10} and EC_{50}, the concentrations that inhibited 10% and 50% of the growth, respectively. (c) Growth of yeast exposed to different Yb concentrations. (d) Growth ratio (OD at 9 h over OD at 4 h) of yeast exposed to increasing amounts of Yb, enabling the identification of the EC_{10} and EC_{50}. (e) Ionome analysis of cells exposed to La at EC_{10}, Yb at EC_{10} and La at the same concentration as that corresponding to Yb EC_{10} (6 µM). Significant differences from the wild-type condition are indicated by different letters (ANOVA, Tukey HSD). Data are the means (±SD) of three independent cultures. (f) Experimental setup of yeast cultures used for RNA-seq and proteomic analyses. Cells were exposed to two concentrations of La and Yb (EC_{10} and EC_{50}) for two exposure durations (1 h and 4 h). Three independent experiments were carried out for each condition.

3.2. Transcriptomic response to different effective concentrations (ECs) of La and Yb

We first aimed to identify the transcriptomic response of yeast cells to two different conditions of a high (EC_{50}) and a low (EC_{10}) toxicity concentration. The transcriptome of *S. cerevisiae* exposed for one hour to La and Yb at their respective EC_{10} and EC_{50} values was analysed (Fig. 1f, Fig. 2). Overall, we identified 1924 differentially expressed genes (DEGs) (applying a fold change (FC) cut-off of ≥ 1.5 and $p < 0.01$) in at least one condition (REE-stressed cells vs control condition).

The direct comparison of gene expression between EC_{50} and EC_{10} for the two REEs identified only a few DEGs (Fig. 2b). When exposed to La, 10 DEGs showed higher expression at EC_{10} than at EC_{50}, while 14 DEGs were upregulated under EC_{50} conditions (Fig. 2b, Table S2). A similar observation was made for Yb. Twenty-two DEGs were more abundant under the EC_{10} condition than under the EC_{50} condition, while this was the case for 13 DEGs under the EC_{50} condition (Fig. 2b, Table S2). We extended the analysis to the entire set of genes that were significantly differentially expressed relative to the control condition ($p < 0.01$). Again, a relatively high similarity of expression patterns existed between the two exposure concentrations, with only a few

differences in the transcriptomic profiles between the EC_{10} and EC_{50} conditions (Fig. 2a, Table S2). In line with our observations, few differences in DEGs between EC_{10} and EC_{50} exposure were obtained for other metals such as Zn, Cd, Cu, Cr and Ag (Jin et al., 2008). For instance, when exposed to these different metals, only 6 DEGs (Cd), 52 DEGs (Cr) and 69 DEGs (Hg) were found to be different between the EC_{10} and EC_{50} conditions.

Given the small number of differences at the transcriptome level between the two tested concentrations and to optimize the number of changes in protein abundance, only the EC_{50} for both La and Yb was used to analyse the time-evolving proteome.

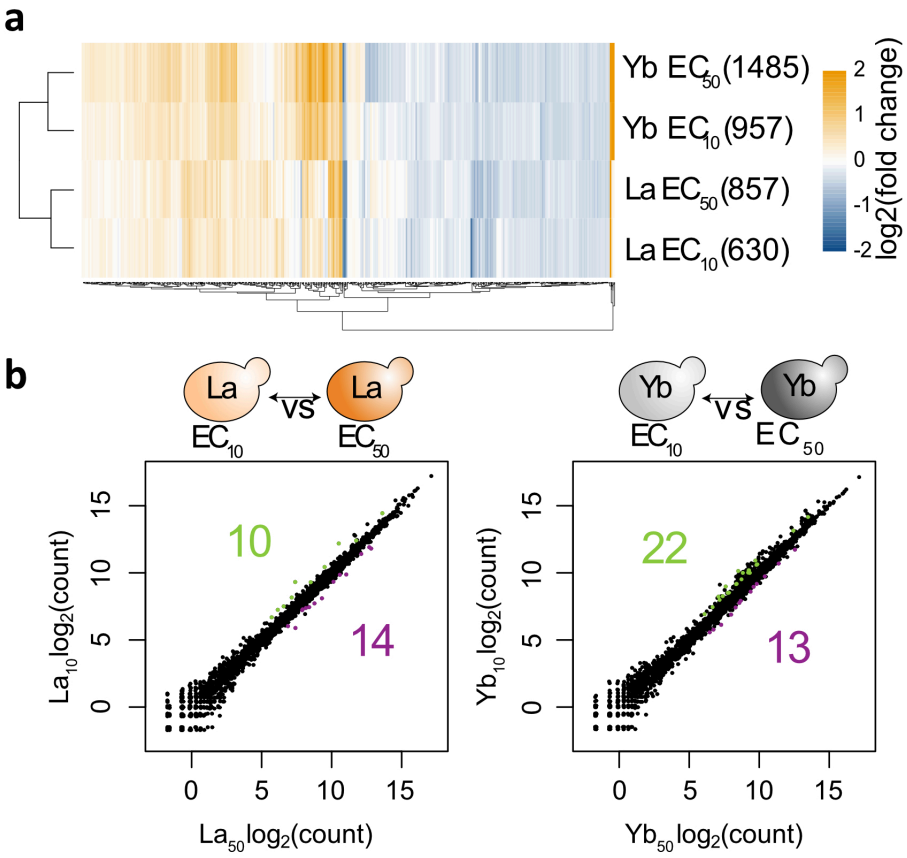

Figure 2. Comparative transcriptomic analyses of yeast exposed to La and Yb showed a similar pattern between the EC_{10} and EC_{50} treatments. (a) Heatmap of differentially expressed genes (DEGs) (blue, downregulated; orange, upregulated) under the two different REE concentrations (EC_{10} and EC_{50} for both La and Yb) in comparison to the control condition. The total number of DEGs ($P \leq 0.01$) is specified in brackets. (b) Scatter plots of DE transcripts under La and Yb exposure. Significantly upregulated and downregulated transcripts ($FC \geq 1.5$, $P \leq 0.01$) are shown in green and purple, respectively.

3.3. Comparative proteomic analysis for two exposure times

Temporal response analysis was performed using a high-throughput shotgun proteomic approach to investigate differences in cellular responses to REEs after short (one hour, representing one generation) and long (four hours, representing 4 generations) exposure times (Fig. 1f). We leveraged label-free proteomic as a semi-quantitative method that quantify peptide peak areas, which allows the direct comparison between samples, unlike label-based methods (iTRAQ, TMT, SILAC). Combining every condition tested and all replicates, a total of 26,785 peptides were detected, as supported by the 685,981 MS/MS spectra. This analysis allowed the successful identification of 2,630 proteins, among which 2,015 were certified and quantified. Identified proteins with significant changes in abundance ($FC \geq 1.5$ and $P \leq 0.05$) upon REE exposure were

used for the analysis. Many more differentially abundant proteins (DAPs) were found at one hour than at four hours in both the La and Yb exposure conditions. As shown in Fig. 3a, 2.6 times more proteins were identified as differentially abundant in the one hour exposure compared to the 4 hour exposure, with total of 161 DAPs at one hour and 62 at four hours under La stress (Fig. 3a, Table S3). Similarly, under Yb stress, 226 and 76 DAPs were found after one and four hours (3 times more), respectively (Fig. 3b, Table S3). Only 10 (La) and 14 (Yb) DAPs were shared between the two exposure times (Fig. 3a-c). These results suggest the establishment of an intense and faster response during a short exposure time relative to durable acclimation after a long exposure time. Similar conclusions were drawn from the direct comparison of DAPs between the one- and four-hour exposure for both REEs. This was also found in a previous study in which *S. cerevisiae* was exposed to other metals (Ag, Cd, Hg, Zn) and metalloids (As) and the transcriptomic response under acute stress (30 min) and sustained stress (2 hours) was compared (Hosiner et al., 2014). Under exposure to these metals, only 2.4% to 7.9% of the total DEGs were shared between the acute and sustained stress (Hosiner et al., 2014). These results further support a time-course adaptation process in yeast cells to cope with toxic metals.

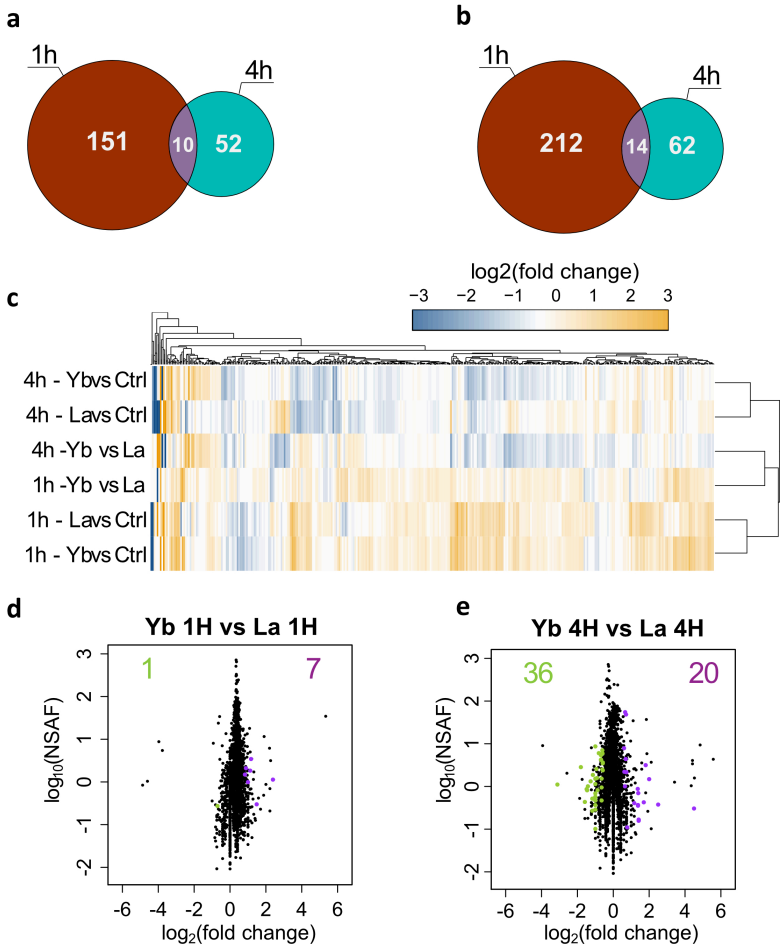

Figure 3. Comparative proteomic analyses of *S. cerevisiae* exposed to La and Yb demonstrate a differential response over time. (a) Venn diagrams of differentially expressed proteins under La exposure vs control conditions after 1 h and 4 h. (b) Same as (a) but for Yb. (c) Heatmap of differentially expressed proteins (blue, downregulated; orange, upregulated) under the two different exposure times (1 h and 4 h). (d) Scatter plot of differentially abundant proteins between Yb and La after 1 hour of exposure. Significantly more abundant proteins under La exposure are shown in green, and those more abundant under Yb are in purple (FC ≥ 1.5, P ≤ 0.05). (e) Same as (d) but after 4 hours. NSAF = normalized spectral abundance factor.

3.4. Combining transcriptomic and proteomic analyses

The proteome analysis of cells exposed for 1 hour to La or Yb allowed the identification of essential genes and the related pathways that cells first activate upon exposure. There was a relatively low number of downregulated proteins under both conditions, with 12 DAPs for La and 7 DAPs for Yb ($FC \geq 1.5$ and $p \leq 0.05$), and these were mainly shared (Table S3, Fig. 3d). Furthermore, these proteins were all involved in ribosome biogenesis (La) and rRNA processing (La) (Tables S4-S6). For all DAPs with a p-value ≤ 0.05, there was high representation of the NOP (nucleolar protein), RPL (ribosomal protein of the large subunit) and RPS (ribosomal protein of the small subunit) family proteins (Table S3). These data further support the downregulation of ribosome biogenesis and consequently less protein synthesis under both La and Yb stress. A reduction in ribosome abundance was reported under different metallic stresses as being a rapid, effective, and reversible stress response to prevent misfolded proteins (Guerra-Moreno et al., 2015; Hosiner et al., 2014; Pimentel et al., 2012; Taymaz-Nikerel et al., 2016; White et al., 1990). Guerra-Moreno et al. (2015) suggested that when cellular ribosome levels are reduced, newly synthesized misfolded proteins may be limited. Lower levels of misfolded proteins would enable proteolysis to more effectively eliminate misfolded proteins (Guerra-Moreno et al., 2015).

In line with this observation, and when considering proteins with increased abundance when exposed to REEs, most of the GO terms represented in the two data sets were proteolysis-related (Tables S4 and S5). In the Yb treatment, an increased abundance of transcripts and proteins belonging to ubiquitin-dependent protein catabolism was also found (Table S7). The short-term exposure of yeast cells to toxic ions appears to trigger a rapid detoxification process by degrading proteins that have been damaged by metal stress. Proteolysis induction is a global cellular response to metallic stress and has been observed at toxic concentrations of Al, Ag, Cd, Mn, Ni, Zn, Hg, and As (Guerra-Moreno et al., 2015; Hosiner et al., 2014; Jin et al., 2008). Additionally, under both treatments, proteins involved in carbohydrate metabolism were more abundant (Tables S4 and S5). Jin et al. (2008) grouped metal-induced biological processes under the term ‘common metal responsive’ genes (Jin et al., 2008). It appears that in response to acute stress (i.e., after one hour of exposure), yeast cells preferentially alleviate toxic effects triggered by the accumulated REEs and then establish adaptation responses to sustained stress (Hosiner et al., 2014).

When comparing the transcriptomic and proteomic profiles at one and four hours for both REEs, the highest correlations were observed between transcriptomic profiles obtained after one hour and proteomic profiles obtained after four hours (Fig. 4a,b, Table S8). Strikingly, there was hardly any overlap between differentially expressed mRNA and the corresponding differentially expressed proteins (Fig. 4c,d). For instance, under La exposure, the expression of 21 of the 30 (70%) more abundant proteins and 28 of the 32 less abundant proteins was not altered for the cognate mRNAs (Fig. 4c). The same observation was found for Yb exposure, with as high as 50% of the proteins with increased abundance and 100% of those with decreased abundance for which the corresponding mRNA was not differentially expressed (Fig. 4d). These observations could be explained by the relatively low number of DAPs ($FC \geq 1.5$ and $P \leq 0.05$) in comparison with the number of DEGs ($FC \geq 1.5$ and $P \leq 0.01$). A fourfold higher number of mRNAs than proteins were differentially expressed under La exposure, while it was 6.4-fold greater under Yb exposure (Fig. 4c,d).

Interestingly, several DAPs and DEGs were shared between the Yb and La treatments, but some were specific to one or the other (Fig. 3e). We thus analysed each data set for the enriched gene ontology (GO terms) to identify modulated pathways and functions in response to either La or Yb (Fig. 5a-d, Tables S9-S13).

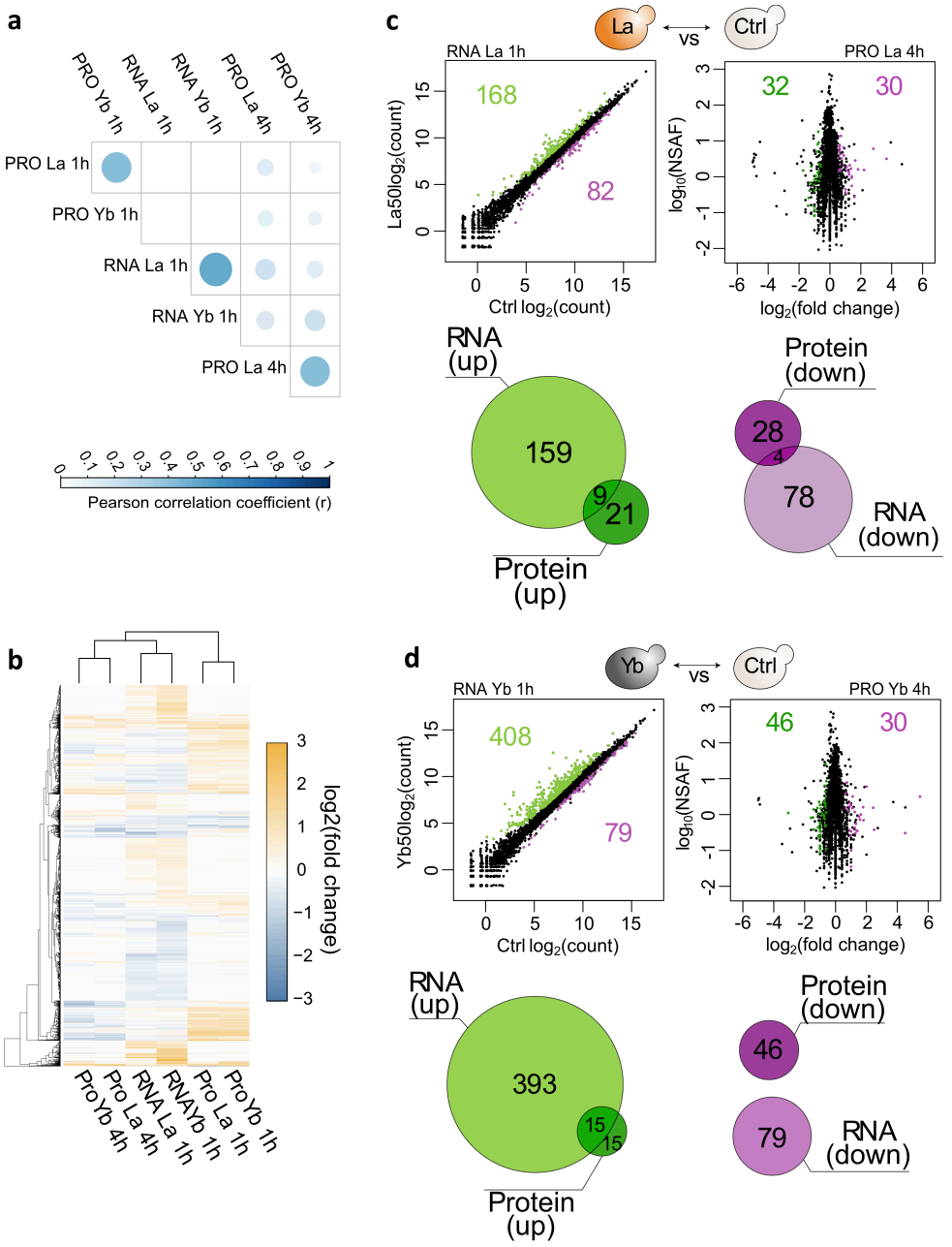

Figure 4. Comparative transcriptomic and proteomic analyses of yeast exposed to REEs at the EC_{50}. (a) Correlation matrix (Pearson's correlation coefficient r) of transcriptomic and proteomic data sets. (b) Heatmap of differentially abundant (DA) proteins (Pro) and differentially expressed (DE) transcripts (RNA) at the different exposure times (1 h and 4 h, as indicated) under La or Yb stress (blue, downregulated; orange, upregulated). (c) Scatter plots and Venn diagrams of DA proteins (after 4 h) and mRNA (after 1 h) under La exposure vs control conditions. Significantly upregulated and downregulated proteins (FC ≥ 1.5, P ≤ 0.05) or transcripts (FC ≥ 1.5, P ≤ 0.01) are shown in green and purple, respectively. (d) Same legend as in (c) under Yb exposure. NSAF = normalized spectral abundance factor.

3.5. The cell wall as the first barrier to REEs

Regarding the response to La at the transcriptomic level, upregulated genes were mainly associated with cell wall biogenesis and organization. These functions were conspicuously represented by four GO terms and associated with up to 31 different genes (Fig. 5a, Table S12). Accordingly, fungal-type cell wall organization was also enriched in the differentially expressed proteins (Fig. 5b, Fig. 4c, Table S9). This finding was supported by the enriched GO cellular compartments (Table S12). Compared to La, Yb exposure upregulated 28 genes involved in fungal-type cell wall

organization and cell wall organization (Fig. 5c, Fig. 4c, Table S7). Moreover, these two functions were also found in the proteomic analysis under Yb stress. This was reinforced by the upregulation of the chitin cell wall metabolic process and the 1,3-β-D-glucan biosynthesis (Fig. 5d, Table S10). Mid2p acts as a sensor for cell wall integrity signalling and activates this pathway. Downstream of the Mid2p signalling pathway, Slt2p, a serine/threonine MAP kinase involved in regulating the maintenance of cell wall integrity, was also upregulated (Fig. 6a). *GSC2* (*FKS2*) is known to be triggered by cell wall stress and encodes a catalytic subunit of 1,3-ß-glucan synthase (Inoue et al., 1995), and it was specifically upregulated under Yb stress. *CWP1* and *NCW2* were upregulated under La and Yb exposure and were identified in the transcriptomic and proteomic analyses (Fig. 6a). Cwp1p is a cell wall mannoprotein linked to a ß-1,3- and ß-1,6-glucan heteropolymer, while Ncw2p is thought to aid the organization of the ß-1,3-glucan structure of the cell wall. These two proteins are needed for the proper organization of cell wall constituents (Lesage and Bussey, 2006; Levin, 2005).

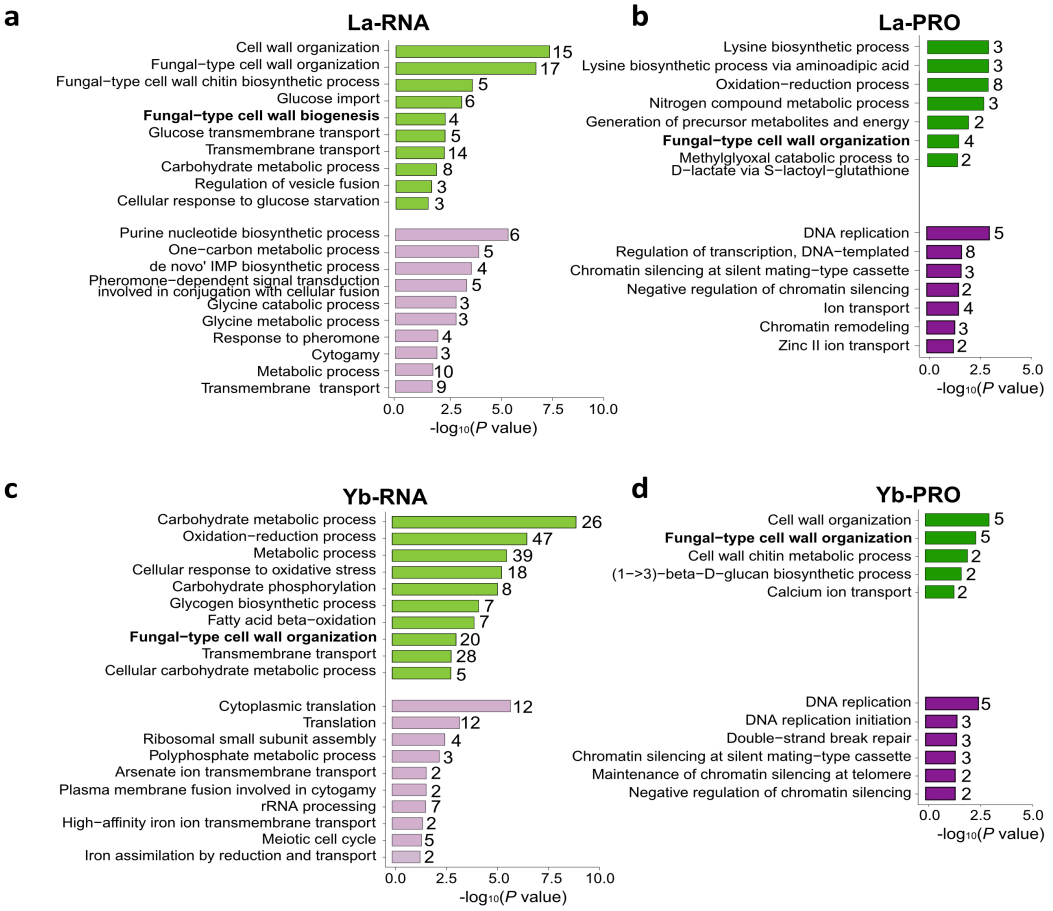

Figure 5. Biological pathway (BP) GO terms overrepresented in the transcriptomic and proteomic analyses of yeast exposed to REEs at the EC_{50}. (a) BP GO terms of DE transcripts under La exposure. (b) BP GO terms of DE proteins under La exposure. (c) BP GO terms of DE transcripts under Yb exposure. (d) BP GO terms of DA proteins under Yb exposure. GO terms significantly enriched in upregulated (green) and downregulated (purple) proteins ($P \leq 0.05$) and transcripts ($P \leq 0.01$). GO terms found in both RNA-seq and proteomic analyses are in bold. Numbers indicate the number of proteins or mRNAs of the specified BP found in the data sets.

The overrepresentation of these cell wall-related biological pathways (BPs) supports the role of this compartment in the first barrier yeast have against REEs. It also provides additional clues about how the different REEs interact with the cell wall (Fig. 7). Ce (Jiang et al., 2010) and Yb (Jiang et

al., 2012) were shown to adsorb to the cell wall of *S. cerevisiae*, *Bacillus subtilis*, and *E. coli*, with affinity differences between LREEs and HREEs (Takahashi et al., 2010).

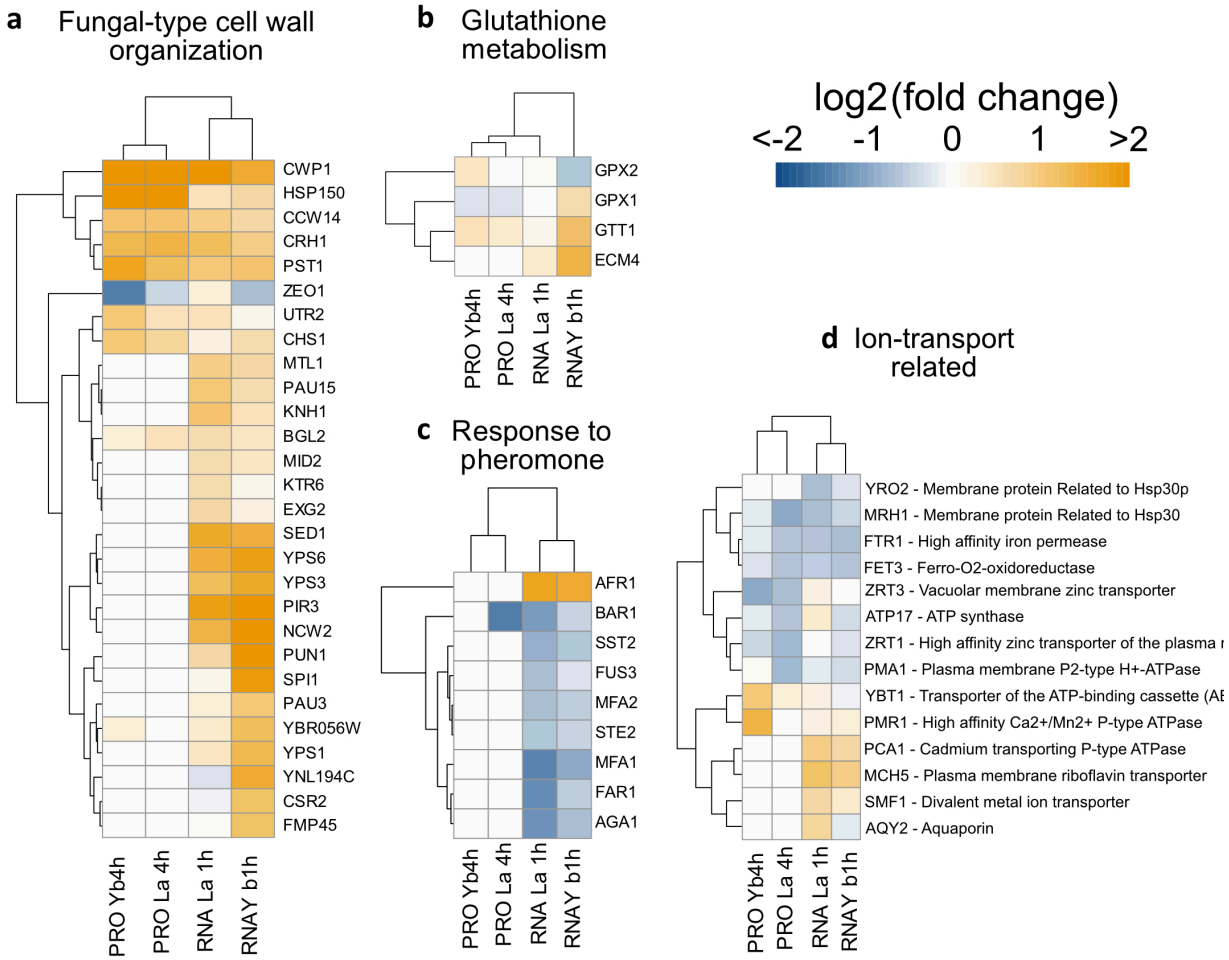

Figure 6. Expression heatmaps of GO terms enriched in proteomic and transcriptomic analyses for both REEs. (a) Fungal-type cell wall organization, (b) Glutathione metabolism, (c) Response to pheromones, (d) Ion transport-related GO terms ($p < 0.05$). The genes and proteins shown were all significantly differentially expressed.

Surface complexation modelling showed that LREEs preferentially associated with phosphate groups, while HREEs associated equally well with carboxyl and phosphate groups. Potentiometric titration and FTIR spectroscopic analyses of *S. cerevisiae* showed a higher representation of phosphate groups (68%) on the cell surface, while amino/hydroxyl (16%) and carboxyl groups (16%) were less represented (Rogowska et al., 2018). The surface of the yeast cell wall, which bears such groups, has been modelled to bind Ca ions, which could potentially be broadened to REEs given their similarities (Rogowska et al., 2018). The higher representation of phosphate groups on the surface and the high affinity of LREEs for these groups could explain the relatively lower toxicity observed for La compared to Yb (Fig. 1). Thus, the upregulation of cell wall-related genes appears to be essential in response to REE exposure and could allow the recycling or selective remodelling of the yeast cell wall to cope with these elements. Modifications of the exposed groups on the surface could ensue, with possible consequences for REE binding. Taken together, these results support the involvement of the cell wall as a primary way in which REEs interact with yeast cells and indicates that there are differences in La- and Yb-triggered effects.

3.6. Involvement of the pheromone signalling pathway

An investigation of the BPs related to sensing the extracellular environment indicated the involvement of pheromone-related GO biological pathways. Indeed, two enriched GO biological pathways were downregulated under La stress, and both were involved in pheromone signalling pheromone-dependent signal transduction (involved with cellular fusion) and the response to the pheromone pathway (Fig. 5a, Fig. 6c, Table S12). Although these GO terms were specifically enriched under La stress, genes belonging to these pathways were also significantly downregulated under Yb stress, but to a lesser extent (Fig. 6c, Table S2). The GO terms included *MFA1* and *MFA2*, the two genes encoding mating pheromone a. The alpha-factor pheromone receptor gene *STE2* and its associated heterotrimeric G protein *SST2* were also downregulated.

Two genes downstream of the regulation cascade triggered by *STE2* were also downregulated: *FAR1* and *FUS3*. *FAR1* is phosphorylated by *FUS3* (a mitogen-activated serine/threonine protein kinase involved in mating) in response to mating pheromone. Several other genes modulated by the pheromone response pathways were also downregulated (Fig. 6c). Prm1p is a pheromone-regulated multispanning membrane protein that is involved in membrane fusion during mating, and Bar1p is an aspartyl protease secreted into the periplasmic space of mating type a cells (Mackay et al., 1988). The latter cleaves and inactivates alpha factor, allowing cells to recover from alpha-factor-induced cell cycle arrest.

There is a possible link between the pheromone response pathway and the REE-triggered response. It is known that some REEs are Ca analogues, particularly La (Fricker and Fricker, 2006) and can be absorbed through the Ca influx system Cch1-Mid1 in yeast cells (Ene et al., 2015). Ca influx occurs during the mating process and is initiated by mating pheromone detection (Carbó et al., 2016; Cunningham, 2011). The response to mating pheromones notably includes increased expression of the high-affinity Ca channels Cch1p-Mid1p and Ecm7p and increased expression of the putative low-affinity Ca channels (Fig. 1p) (Cunningham, 2011; Muller et al., 2003). Thus, considering that REEs can pass through Ca channels, the downregulation of pathways involved in the transcription of these channels would reduce the amount of REEs in the cytoplasm. However, such a hypothesis requires further investigation of whether REE accumulation modifies pheromone metabolism. In response to pheromones, yeast cells modify their cell wall to allow fusion with cells of the other mating type, but they also induce cell cycle arrest (Chen and Thorner, 2007), thereby leading to a more susceptible cell wall. Therefore, in line with previous observations, the downregulation of genes and proteins involved in the pheromone-dependent signal transduction pathway could reduce cell cycle arrest and cell wall alteration processes, allowing cells to better cope with La and Yb toxicity (Fig. 7).

3.7. Lanthanum and ytterbium impact amino acid, carbohydrate, and DNA metabolism

Under La stress, several metabolic and biosynthetic processes were altered at the transcriptomic and proteomic levels (Fig. 5a, Table S12). The biosynthesis of purine nucleotides, through de novo IMP (Fig. 5a) and AMP biosynthetic processes was significantly downregulated. Additionally downregulated was the one-carbon metabolic process, which is related to glycine metabolism (Fig. 5a, Table S12). Conversely, the proteomic analysis demonstrated that lysine biosynthesis was upregulated (10%) under La stress (Fig. 5b, Table S9). Interestingly, other than three upregulated genes involved in proline transmembrane transport, no other amino acid-related GO terms were identified under Yb stress (Fig. 5c, d, Table S7).

A relatively high number of upregulated genes were associated with carbohydrate metabolism under both treatments, with eight upregulated genes under La stress and 26 under Yb stress (Fig. 5a,c). Many carbohydrate-related GO terms were enriched in the Yb condition, highlighting the

involvement of this pathway in the response to Yb. However, the induction of carbohydrate metabolism was reported to be a common metal-responsive pathway and was also found when yeast cells were exposed to several other toxic metals (Jin et al., 2008).

The two analytical methods identified *INO1* and its encoded protein Ino1p as the most upregulated representatives under both La and Yb exposure (Table S8). The inositol-3-phosphate synthase Ino1p is involved in the synthesis of inositol phosphates and inositol-containing phospholipids. Under phosphate limitation conditions, genes implicated in inositol phosphate uptake and metabolism, phosphate metabolism, and metabolite phosphorylation were induced (Taymaz-Nikerel et al., 2016). It has recently been shown that inositol-3-phosphates are involved in the localization of metal uptake transporters in *Arabidopsis thaliana* (Agorio et al., 2017). Thus, an increase in inositol-3-phosphate through the upregulation of *INO1* could be important for membrane transporter localization in response to REEs. Another explanation would be that increased inositol phosphates help to chelate REEs, thus decreasing their toxicity and reactivity. Indeed, all inositol phosphates are strong chelators of metal ions such as Ca, Mg, Zn, Cu, Fe, Mn and Al (Chastukhina and Sharipova, 2014; Oh et al., 2006).

Finally, aside from the ion transport-related GO terms for La, almost all downregulated proteomic pathways for both REEs were related to DNA replication and regulation (Fig. 5b,d, Tables S9, S10). Proteins involved in DNA replication were downregulated under both La and Yb exposure, and proteins involved in transcription regulation were downregulated under La exposure. Yb stress also reduced translation, RNA processing and ribosome small subunit assembly at the transcriptomic level (Fig. 5c). It has been strongly suggested that DNA replication is a target for Cd toxicity (Serero et al., 2008). The downregulation of DNA replication by La and Yb could be evidence of toxicity targets similar to Cd.

3.8. Ytterbium triggers oxidative stress response

In Yb-exposed yeast, the most represented process was the GO term oxidation-reduction (47 genes) (Fig. 5c Table S7). In addition, 18 genes involved with the cellular response to oxidative stress were also upregulated, suggesting that Yb triggers oxidative stress and NADPH regeneration (Fig. 5c, Table S7). While only seen with the Yb stress in our study, it has been extensively shown that other REEs can also generate oxidative stress (Gonzalez et al., 2014; Liang and Wang, 2013; Pagano et al., 2015). Several genes involved in glutathione (GSH) homeostasis were upregulated specifically under Yb stress. GSH can act at three different levels. First, GSH can chelate toxic metals to form a complex that can subsequently be sequestered into the vacuole. GSH can also act as a protective agent against metal-induced oxidation (Jozefczak et al., 2012). Finally, protein glutathionylation can occur, resulting in a protective role against irreversible metal binding and/or oxidative damage to proteins (Deponte, 2017; Wysocki and Tamás, 2010).

Among the upregulated genes involved in GSH homeostasis under Yb stress, we identified *GTT1* (ER) and *ECM4* (*GTO2*, cytoplasm), and, to a lesser extent, *GRX1* (cytosol) and *GRX2* (cytosol and mitochondria) (Fig. 6b, Table S2). Gtt1p and Ecm4p are glutathione-S-transferases (GSTs), while Grx1p and Grx2p are glutaredoxins that can fill the same role as GSTs (Morano et al., 2012). GSTs catalyse the conjugation of GSH with a substrate (e.g., Cd) or the isomerization of GSH to form oxidized glutathione (Daniela et al., 2009). Furthermore, the upregulation of the gene encoding the gamma-glutamyltranspeptidase *ECM38* (Table S2), a major glutathione-degrading enzyme localized into the vacuole, suggests the translocation of oxidized glutathione into the vacuole, with a subsequent need for recycling (Cordente et al., 2015). Thus, along with ROS production inducing oxidative stress, Yb could be internalized through GSH-Yb complexes via the vacuole (Fig. 7). The ABC transporter Ybf1p, which was more abundant under Yb exposure, might

be involved in this process (Fig. 6d). This latter hypothesis requires further investigation to verify the involvement of glutathione in Yb detoxification.

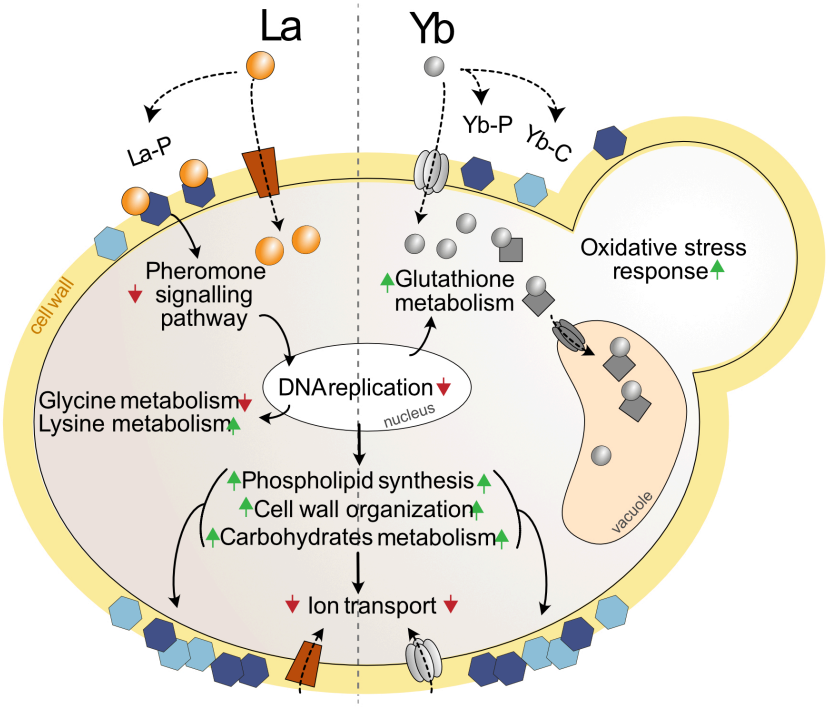

Figure 7. Schematic model of detoxification responses in yeast under acute REE stress. Upregulated functions are indicated by a green arrow, while downregulated functions are indicated by a red arrow. La-P and Yb-P correspond to phosphate-bound REEs, while Yb-C corresponds to carboxylate-bound Yb. Grey squares represent putative ligands that bind HREEs. Dashed arrows indicate REE movement, and plain arrows indicate response mechanisms.

3.9. Lanthanum and ytterbium affect plasma membrane transport

Reducing the import of toxic ions into the cell is another mechanism by which cells can adapt to xenobiotic compounds. Of the downregulated genes under Yb and La exposure, several were linked to plasma membrane ion transport (Fig. 7). Under Yb exposure, three transport-related GO terms were enriched: arsenate ion transmembrane transport, high-affinity Fe ion transmembrane transport and Fe assimilation by reduction and transport (Fig. 5c, Table S7). Under La exposure, four downregulated proteins were involved in ion transport, and two of these were related to Zn ion transport (Fig. 5b, Table S12). Regarding ion transport GO terms, the two genes encoding the two components of the high-affinity Fe transport system Fet3p-Ftr1p were downregulated under both La and Yb exposure (Fig. 6d). A similar finding was identified at the protein level. Fet3p is a multicopper oxidase that oxidizes ferrous Fe to ferric Fe for subsequent cellular uptake by the transmembrane permease Ftr1p (Stearman et al., 1996). Other ion transport-related genes and proteins also had modified expression, as evidenced by transcriptomic or proteomic analyses (Fig. 6d). Along with Fet3-Ftr1, the plasma membrane high-affinity Zn transporter Zrt1p was also downregulated in the presence of both REEs (Fig. 6d). Also downregulated was the Zn transporter Zrt3p, which localizes to the vacuolar membrane (Fig. 6d, Table S8). Zrt3p transports Zn ions from vacuolar storage to the cytoplasm. Conversely, some genes encoding transmembrane ion transporters were upregulated. Among them were *PCA1*, encoding a cadmium efflux transporter, and *SMF1*, encoding a divalent metal transporter. A closer investigation of the roles played by these different metal transport systems would help to elucidate novel REE uptake pathways in yeast cells. Furthermore, the modulated expression and abundance of these nutrient transporters could

be the result of REEs indirectly impacting the overall nutrient balance in cells. Interestingly, we observed an overall increase of the cell content of several cations (Fig. 1e) that might be a result of a partial membrane permeabilization by REEs (Ramos et al., 2016; Técher et al., 2020), triggering a stress response illustrated by the higher abundance of Hog1p, and higher expression of *ENA1* encoding a Na efflux system (Haro et al., 1991) in response to Yb (Tables S2-S3). The Hog1p MAPK pathway is involved in the response to high osmolarity and has been hypothesized to take part in the tolerance to As and other metals (Hosiner et al., 2014). However, this Hog1p mediated stress response is likely due to the plasma membrane permeability induced by REEs rather than an hyperosmolarity given the very low REE concentration used. In response to this uncontrolled ion influx, metal-homeostasis mechanisms would be triggered to reduce metal uptake by inhibiting metal transporters expression and translation. Additionally, high concentration of toxic metals such as Cd downregulate the expression of the zinc transporter Zrt1p to prevent uptake of toxic Cd (Gitan et al., 1998; Wysocki and Tamás, 2010). The high concentrations of REEs could also contribute to this deregulation of membrane influx systems. The altered Fe and Zn homeostasis under La or Yb stresses could rapidly be alleviated by downregulating the corresponding uptake systems (Fet3p-Ftr1p, Zrt1p and Zrt3p) to reduce Fe and Zn loading into the cytosol.

4. Conclusion

Here, we report the first cellular and molecular insights into the REE toxicity response in the eukaryotic model organism *S. cerevisiae*. The use of complementary methods at different levels of regulation (mRNA and protein) has furthered our understanding of the potential issues related to these emerging metal contaminants. Some responses have previously been shown for other toxic elements, such as Cd. Among these shared responses, proteolysis, ribosome biogenesis regulation, and oxidative stress were specific to Yb and were not seen for La. However, other pathways and compartments appeared to be important for detoxification and/or the avoidance of the toxic impacts of La and Yb. Unlike the toxicity triggered by other metals, here we found that the cell wall and pheromone signalling pathways were key response pathways for yeast cells exposed to La and Yb (Fig. 7). Interestingly, several differences were observed between La (LREE) and Yb (HREE) exposure, indicating the heterogeneity of impacts and responses triggered by REEs. Other toxic metals, such as Cd, can be taken up through Zrt1p, Smf1p, Fet4p and Mid1p (Wysocki and Tamás, 2010). We found in the present study previously unidentified mechanisms of nonspecific REE entry into the cytosol through different transporters. Taken together, these findings provide valuable information at the cellular and molecular levels to better assess the impacts and behaviour of REEs towards eukaryotic organisms.

Credit authorship contribution statement

Nicolas Grosjean: Methodology, Data acquisition, Data curation and treatment, Data analysis, Writing - original draft, review & editing. **Marie Le Jean, Damien Blaudez**: Conceptualization, Methodology, Formal analysis, Funding acquisition, Supervision, Writing - review & editing. **Jean Armengaud**: Proteomics data acquisition. **Michel Chalot**: Data acquisition, Writing - review & editing. **Adam Schikora, Elisabeth M. Gross**: Writing - review & editing.

Declaration of Competing Interest

The authors declare that they have no known competing financial interests or personal relationships that could have appeared to influence the work reported in this paper.

Acknowledgements

This work has been supported by the French National Research Agency through the national program 'Investissements d'avenir' with the reference ANR-10-LABX-21-01/LABEX RESSOURCES21 and by the Région Grand Est.

Conflicts of interest

Authors have no conflicts of interest to declare.

References

Agorio, A., Giraudat, J., Bianchi, M.W., Marion, J., Espagne, C., Castaings, L., Lelièvre, F., Curie, C., Thomine, S., Merlot, S., 2017. Phosphatidylinositol 3-phosphate-binding protein AtPH1 controls the localization of the metal transporter NRAMP1 inArabidopsis. Proc. Natl. Acad. Sci. U. S. A. 114, E3354–E3363. https://doi.org/10.1073/pnas.1702975114

Babula, P., Klejdus, B., Kovacik, J., Hedbavny, J., Hlavna, M., 2015. Lanthanum rather than cadmium induces oxidative stress and metabolite changes in Hypericum perforatum. J. Hazard. Mater. 286, 334–342.

Binnemans, K., Jones, P.T., Blanpain, B., Van Gerven, T., Yang, Y., Walton, A., Buchert, M., 2013. Recycling of rare earths: A critical review. J. Clean. Prod. 51, 1–22. https://doi.org/10.1016/j.jclepro.2012.12.037

Botstein, D., Chervitz, S.A., Cherry, J.M., 1997. Yeast as a model organism. Science (80-.). 277, 1259–1260. https://doi.org/10.1126/science.277.5330.1259

Carbó, N., Tarkowski, N., Ipiña, E.P., Dawson, S.P., Aguilar, P.S., 2016. Sexual pheromone modulates the frequency of cytosolic Ca2+ bursts in Saccharomyces cerevisiae. Mol. Biol. Cell 28, 1–26. https://doi.org/https://doi.org/10.1091/mbc.e16-07-0481

Carvalho, P.C., Yates, J.R., Barbosa, V.C., 2012. Improving the TFold test for differential shotgun proteomics. Bioinformatics 28, 1652–1654. https://doi.org/10.1093/bioinformatics/bts247

Chastukhina, I.B., Sharipova, M.R., 2014. Inositol Phosphates and their Biological Effects 7, 433–437.

Chen, R.E., Thorner, J., 2007. Function and regulation in MAPK signaling pathways: Lessons learned from the yeast Saccharomyces cerevisiae. Biochim. Biophys. Acta - Mol. Cell Res. 1773, 1311–1340. https://doi.org/10.1016/j.bbamcr.2007.05.003

Ciacci, L., Reck, B.K., Nassar, N.T., Graedel, T.E., 2015. Lost by design. Environ. Sci. Technol. 49, 9443–9451. https://doi.org/10.1021/es505515z

Cordente, A.G., Capone, D.L., Curtin, C.D., 2015. Unravelling glutathione conjugate catabolism in Saccharomyces cerevisiae : the role of glutathione / dipeptide transporters and vacuolar function in the release of volatile sulfur compounds 3-mercaptohexan-1-ol and 4-mercapto-4-methylpentan-2-one. Appl. Microbiol. Biotechnol. https://doi.org/10.1007/s00253-015-6833-5

Cotton, S., 2006. Lanthanide and Actinide Chemistry, John Wiley. ed. https://doi.org/10.1002/0470010088

Cunningham, K.W., 2011. Acidic calcium stores of Saccharomyces cerevisiae. Cell Calcium 50, 129–138. https://doi.org/10.1016/j.ceca.2011.01.010

Daniela, P., Adamis, B., Mannarino, S.C., Cristina, E., Eleutherio, A., 2009. Glutathione and gamma-glutamyl transferases are involved in the formation of cadmium – glutathione complex. FEBS Lett. 583, 1489–1492. https://doi.org/10.1016/j.febslet.2009.03.066

Deponte, M., 2017. The Incomplete Glutathione Puzzle : Just Guessing at Numbers and Figures ? 27, 1130–1161. https://doi.org/10.1089/ars.2017.7123

Dupierris, V., Masselon, C., Court, M., Kieffer-Jaquinod, S., Bruley, C., 2009. A toolbox for validation of mass spectrometry peptides identification and generation of database: IRMa. Bioinformatics 25, 1980–1981. https://doi.org/10.1093/bioinformatics/btp301

El-Ramady, H.R.H., 2008. A contribution on the bio-actions of rare earth elements in the soil / plant environment. Technischen Universität Carolo-Wilhelmina zu Braunschweig.

Ene, C.D., Ruta, L.L., Nicolau, I., Popa, C. V., Iordache, V., Neagoe, A.D., Farcasanu, I.C., 2015. Interaction between lanthanide ions and Saccharomyces cerevisiae cells. JBIC J. Biol. Inorg. Chem. 20, 1097–1107. https://doi.org/10.1007/s00775-015-1291-1

Fitriyanto, N.A., Nakamura, M., Muto, S., Kato, K., Yabe, T., Iwama, T., Kawai, K., Pertiwiningrum, A., 2011. Ce 3 + -induced exopolysaccharide production by Bradyrhizobium sp . MAFF211645. JBIOSC 111, 146–152. https://doi.org/10.1016/j.jbiosc.2010.09.008

Fricker, S.P., Fricker, S., 2006. The therapeutic application of lanthanides. https://doi.org/10.1039/b509608c

Gao, J., Li, R., Wang, F., Liu, X., Zhang, J., Hu, L., Shi, J., He, B., Zhou, Q., Song, M., Zhang, B., Qu, G., Liu, S., Jiang, G., 2017. Determining the Cytotoxicity of Rare Earth Element Nanoparticles in Macrophages and the Involvement of Membrane Damage. Environ. Sci. Technol. 51, 13938–13948. https://doi.org/10.1021/acs.est.7b04231

Gitan, R.S., Luo, H., Rodgers, J., Broderius, M., Eide, D., 1998. Zinc-induced inactivation of the yeast ZRT1 zinc transporter occurs through endocytosis and vacuolar degradation. J. Biol. Chem. 273, 28617–28624. https://doi.org/10.1074/jbc.273.44.28617

Gonzalez, V., Vignati, D.A.L., Leyval, C., Giamberini, L., 2014. Environmental fate and ecotoxicity of lanthanides: Are they a uniform group beyond chemistry? Environ. Int. 71, 148–157. https://doi.org/10.1016/j.envint.2014.06.019

Grosjean, N., Blaudez, D., Chalot, M., Gross, E.M., Le Jean, M., 2020. Identification of new hardy ferns that preferentially accumulate light rare earth elements: A conserved trait within fern species. Environ. Chem. 17, 191–200. https://doi.org/10.1071/EN19182

Grosjean, N., Gross, E.M., Le Jean, M., Blaudez, D., 2018. Global deletome profile of Saccharomyces cerevisiae exposed to the technology-critical element yttrium. Front. Microbiol. 9, 1–13. https://doi.org/10.3389/fmicb.2018.02005

Grosjean, N., Le Jean, M., Berthelot, C., Chalot, M., Gross, E.M., Blaudez, D., 2019. Accumulation and fractionation of rare earth elements are conserved traits in the Phytolacca genus. Sci. Rep. 9, 18458. https://doi.org/10.1038/s41598-019-54238-3

Guerra-Moreno, A., Isasa, M., Bhanu, M.K., Waterman, D.P., Eapen, V. V., Gygi, S.P., Hanna, J., 2015. Proteomic analysis identifies ribosome reduction as an effective proteotoxic stress response. J. Biol. Chem. 290, 29695–29706. https://doi.org/10.1074/jbc.M115.684969

Gwenzi, W., Mangori, L., Danha, C., Chaukura, N., Dunjana, N., Sanganyado, E., 2018. Sources , behaviour , and environmental and human health risks of high- technology rare earth elements as emerging contaminants. Sci. Total Environ. 636, 299–313. https://doi.org/10.1016/j.scitotenv.2018.04.235

660 Haro, R., Garciadeblas, B., Rodriguez-Navarro, A., 1991. A novel P-type ATPase from yeast
661 involved in sodium transport. FEBS Lett. 291, 189–191. https://doi.org/10.1016/0014-
662 5793(91)81280-L
663 Hartmann, E.M., Allain, F., Gaillard, J., Pible, O., Armengaud, J., 2014. Taking the Shortcut for High-
664 Throughput Shotgun Proteomic Analysis of Bacteria, in: Vergunst, A., O'Callaghan, D. (Eds.),
665 Host-Bacteria Interactions. Methods in Molecular Biology (Methods and Protocols). Humana
666 Press, New York, NY. https://doi.org/10.1007/978-1-4939-1261-2
667 He, M.L., Rambeck, W.A., 2000. Rare earth elements - A new generation of growth promoters for
668 pigs? Arch. Anim. Nutr. 53, 323–334. https://doi.org/10.1080/17450390009381956
669 He, M.L., Ranz, D., Rambeck, W.A., 2001. Study on the performance enhancing effect of rare earth
670 elements in growing and fattening pigs. J. Anim. Physiol. Anim. Nutr. (Berl). 85, 263–270.
671 https://doi.org/10.1046/j.1439-0396.2001.00327.x
672 Hosiner, D., Gerber, S., Lichtenberg-Fraté, H., Glaser, W., Schüller, C., Klipp, E., 2014. Impact of
673 acute metal stress in Saccharomyces cerevisiae. PLoS One 9, 1–14.
674 https://doi.org/10.1371/journal.pone.0083330
675 Hu, Z., Richter, H., Sparovek, G., Schnug, E., 2004. Physiological and Biochemical Effects of Rare
676 Earth Elements on Plants and Their Agricultural Significance: A Review. J. Plant Nutr. 27, 183–
677 220. https://doi.org/10.1081/PLN-120027555
678 Huang, D.W., Sherman, B.T., Lempicki, R.A., 2009a. Systematic and integrative analysis of large
679 gene lists using DAVID bioinformatics resources. Nat. Protoc. 4.
680 https://doi.org/10.1038/nprot.2008.211
681 Huang, D.W., Sherman, B.T., Lempicki, R.A., 2009b. Bioinformatics enrichment tools : paths
682 toward the comprehensive functional analysis of large gene lists. Nucleic Acids Res. 37, 1–
683 13. https://doi.org/10.1093/nar/gkn923
684 Inoue, S.B., Takewaki, N., Takasuka, T., Mio, T., Adachi, M., Fujii, Y., Miyamoto, C., 1995.
685 Characterization and gene cloning of 1,3-b-D-glucan synthase from Saccharomyces
686 cerevisiae. Eur. J. Biochem. 231, 845–854.
687 Jiang, M., Ohnuki, T., Kozai, N., Tanaka, K., Suzuki, Y., Sakamoto, F., Kamiishi, E., Utsunomiya, S.,
688 2010. Biological nano-mineralization of Ce phosphate by Saccharomyces cerevisiae. Chem.
689 Geol. 277, 61–69. https://doi.org/10.1016/j.chemgeo.2010.07.010
690 Jiang, M.Y., Ohnuki, T., Tanaka, K., Kozai, N., Kamiishi, E., Utsunomiya, S., 2012. Post-adsorption
691 process of Yb phosphate nano-particle: Formation by Saccharomyces cerevisiae. Geochim.
692 Cosmochim. Acta 93, 30–46. https://doi.org/10.1016/j.gca.2012.06.016
693 Jin, Y.H., Dunlap, P.E., McBride, S.J., Al-Refai, H., Bushel, P.R., Freedman, J.H., 2008. Global
694 transcriptome and deletome profiles of yeast exposed to transition metals. PLoS Genet. 4.
695 https://doi.org/10.1371/journal.pgen.1000053
696 Jozefczak, M., Remans, T., Vangronsveld, J., Cuypers, A., 2012. Glutathione is a key player in metal-
697 induced oxidative stress defenses. Int. J. Mol. Sci. https://doi.org/10.3390/ijms13033145
698 Kachroo, A.H., Laurent, J.M., Yellman, C.M., Meyer, A.G., Wilke, C.O., Marcotte, E.M., 2017.
699 Systematic humanization of yeast genes reveals conserved functions and genetic modularity.
700 Science (80-.). 348, 921–925. https://doi.org/10.1016/j.antiviral.2015.06.014.Chronic
701 Klein, G., Mathé, C., Biola-Clier, M., Devineau, S., Drouineau, E., Hatem, E., Marichal, L., Alonso,
702 B., Gaillard, J.C., Lagniel, G., Armengaud, J., Carrière, M., Chédin, S., Boulard, Y., Pin, S.,
703 Renault, J.P., Aude, J.C., Labarre, J., 2016. RNA-binding proteins are a major target of silica

704 nanoparticles in cell extracts. Nanotoxicology 10, 1555–1564.
705 https://doi.org/10.1080/17435390.2016.1244299
706 Lee, J.C.K., Wen, Z., 2018. Pathways for greening the supply of rare earth elements in China. Nat.
707 Sustain. 1, 598–605.
708 Leeuw, D., Academic, K., 2000. Inorganic yellow-red pigments without toxic metals. Nature 404,
709 980–982.
710 Lesage, G., Bussey, H., 2006. Cell Wall Assembly in Saccharomyces cerevisiae. Microbiol. Mol. Biol.
711 Rev. 70, 317–343. https://doi.org/10.1128/MMBR.00038-05
712 Levin, D.E., 2005. Cell Wall Integrity Signaling in Saccharomyces cerevisiae Cell. Microbiol Mol Biol
713 Rev 69, 262–291. https://doi.org/10.1128/MMBR.69.2.262
714 Liang, C., Wang, W., 2013. Antioxidant response of soybean seedlings to joint stress of lanthanum
715 and acid rain. https://doi.org/10.1007/s11356-013-1776-9
716 Mackay, V.L., Welch, S.K., Insley, M.Y., Manneyt, T.R., Holly, J., Saari, G.C., Parker, M.L., 1988. The
717 Saccharomyces cerevisiae BAR1 gene encodes an exported protein with homology to pepsin.
718 Proc. Nati. Acad. Sci. USA 85, 55–59.
719 Morano, K.A., Grant, C.M., Moye-rowley, W.S., 2012. The Response to Heat Shock and Oxidative
720 Stress in Saccharomyces cerevisiae. Genetics 190, 1157–1195.
721 https://doi.org/10.1534/genetics.111.128033
722 Muller, E.M., Mackin, N.A., Erdman, S.E., Cunningham, K.W., 2003. Fig1p facilitates Ca2+ influx
723 and cell fusion during mating of Saccharomyces cerevisiae. J. Biol. Chem. 278, 38461–38469.
724 https://doi.org/10.1074/jbc.M304089200
725 Noack, C.W., Dzombak, D.A., Karamalidis, A.K., 2014. Rare earth element distributions and trends
726 in natural waters with a focus on groundwater. Environ. Sci. Technol. 48, 4317–4326.
727 Oh, B., Kim, M.H., Yun, B., Choi, W., Park, S., Bae, S., Oh, T., 2006. Ca 2 + -Inositol Phosphate
728 Chelation Mediates the Substrate Specificity of -Propeller 9531–9539.
729 Pagano, G., Guida, M., Siciliano, A., Oral, R., Koçbaş, F., Palumbo, A., Castellano, I., Migliaccio, O.,
730 Thomas, P.J., Trifuoggi, M., 2016. Comparative toxicities of selected rare earth elements: Sea
731 urchin embryogenesis and fertilization damage with redox and cytogenetic effects. Environ.
732 Res. 147, 453–460. https://doi.org/10.1016/j.envres.2016.02.031
733 Pagano, G., Guida, M., Tommasi, F., Oral, R., 2015. Health effects and toxicity mechanisms of rare
734 earth elements—Knowledge gaps and research prospects. Ecotoxicol. Environ. Saf. 115, 40–
735 48. https://doi.org/10.1016/j.ecoenv.2015.01.030
736 Panichev, A.M., 2015. Rare Earth Elements: Review of Medical and Biological Properties and Their
737 Abundance in the Rock Materials and Mineralized Spring Waters in the Context of Animal
738 and Human Geophagia Reasons Evaluation. Achiev. Life Sci. 9, 95–103.
739 https://doi.org/10.1016/j.als.2015.12.001
740 Pimentel, C., Vicente, C., Menezes, R.A., Caetano, S., Carreto, L., Rodrigues-Pousada, C., 2012. The
741 role of the Yap5 transcription factor in remodeling gene expression in response to Fe
742 bioavailability. PLoS One 7, 1–11. https://doi.org/10.1371/journal.pone.0037434
743 Ramos, S.J., Dinali, G.S., Oliveira, C., Martins, G.C., Moreira, C.G., Siqueira, J.O., Guilherme, L.R.G.,
744 2016. Rare Earth Elements in the Soil Environment 28–50. https://doi.org/10.1007/s40726-
745 016-0026-4
746 Rim, K.T., Koo, K.H., Park, J.S., 2013. Toxicological Evaluations of Rare Earths and Their Health
747 Impacts to Workers: A Literature Review. Saf. Health Work 4, 12–26.

https://doi.org/10.5491/SHAW.2013.4.1.12
Rogowska, A., Pomastowski, P., Złoch, M., Railean-Plugaru, V., Król, A., Rafińska, K., Szultka-Młyńska, M., Buszewski, B., 2018. The influence of different pH on the electrophoretic behaviour of Saccharomyces cerevisiae modified by calcium ions. Sci. Rep. 8, 2–11. https://doi.org/10.1038/s41598-018-25024-4
Serero, A., Lopes, J., Nicolas, A., Boiteux, S., 2008. Yeast genes involved in cadmium tolerance : Identification of DNA replication as a target of cadmium toxicity. DNA Repair (Amst). 7, 1262–1275. https://doi.org/10.1016/j.dnarep.2008.04.005
Setua, S., Menon, D., Asok, A., Nair, S., Koyakutty, M., 2010. Folate receptor targeted, rare-earth oxide nanocrystals for bi-modal fluorescence and magnetic imaging of cancer cells. Biomaterials 31, 714–729. https://doi.org/10.1016/j.biomaterials.2009.09.090
Souza, I.C., Morozesk, M., Azevedo, V.C., Mendes, V.A.S., Duarte, I.D., Rocha, L.D., Matsumoto, S.T., Elliott, M., Baroni, M. V, Wunderlin, D.A., others, 2021. Trophic transfer of emerging metallic contaminants in a neotropical mangrove ecosystem food web. J. Hazard. Mater. 408, 124424.
Stearman, R., Yuan, D.S., Yamaguchi-lwai, Y., Klausner, R.D., Dancis, A., 1996. A Permease-Oxidase Complex Involved in High-Affinity lron Uptake in Yeast. Science (80-.). 271.
Takahashi, Y., Yamamoto, M., Yamamoto, Y., Tanaka, K., 2010. EXAFS study on the cause of enrichment of heavy REEs on bacterial cell surfaces. Geochim. Cosmochim. Acta 74, 5443–5462. https://doi.org/10.1016/j.gca.2010.07.001
Taymaz-Nikerel, H., Cankorur-Cetinkaya, A., Kirdar, B., 2016. Genome-Wide Transcriptional Response of Saccharomyces cerevisiae to Stress-Induced Perturbations. Front. Bioeng. Biotechnol. 4. https://doi.org/10.3389/fbioe.2016.00017
Técher, D., Grosjean, N., Sohm, B., Blaudez, D., Le Jean, M., 2020. Not merely noxious? Time-dependent hormesis and differential toxic effects systematically induced by rare earth elements in Escherichia coli. Environ. Sci. Pollut. Res. 27, 5640–5649. https://doi.org/10.1007/s11356-019-07002-z
Trifuoggi, M., Pagano, G., Guida, M., Palumbo, A., Siciliano, A., Gravina, M., Lyons, D.M., Burić, P., Levak, M., Thomas, P.J., Giarra, A., Oral, R., 2017. Comparative toxicity of seven rare earth elements in sea urchin early life stages. Environ. Sci. Pollut. Res. 24, 20803–20810. https://doi.org/10.1007/s11356-017-9658-1
Wakabayashi, T., Ymamoto, A., Kazaana, A., Nakano, Y., Nojiri, Y., Kashiwazaki, M., 2016. Antibacterial, Antifungal and Nematicidal Activities of Rare Earth Ions. Biol. Trace Elem. Res. 174, 464–470. https://doi.org/10.1007/s12011-016-0727-y
Wang, L., He, J., Xia, A., Cheng, M., Yang, Q., Du, C., Wei, H., Huang, X., Zhou, Q., 2017. Toxic effects of environmental rare earth elements on delayed outward potassium channels and their mechanisms from a microscopic perspective. Chemosphere 181, 690–698. https://doi.org/10.1016/j.chemosphere.2017.04.141
Wei, B., Li, Y., Li, H., Yu, J., Ye, B., Liang, T., 2013. Rare earth elements in human hair from a mining area of China. Ecotoxicol. Environ. Saf. 96, 118–123. https://doi.org/10.1016/j.ecoenv.2013.05.031
Weiwei, H., Shihua, S., Peidong, T., 2007. Analysis of Inhibitory Effect of Gadolinium on Sinorhizobium fredii. J. Radioanal. Nucl. Chem. 106–110.
White, T.J., Bruns, T., Lee, S., Taylor, J., 1990. Amplification and direct sequencing of fungal

ribosomal RNa genes for phylogenetics., in: Innis, M., Gelfand, D., Sninsky, J., White, T. (Eds.), PCR-Protocol and Applications - a Laboratory Manual. pp. 315–322.
Wysocki, R., Tamás, M.J., 2010. How Saccharomyces cerevisiae copes with toxic metals and metalloids. FEMS Microbiol. Rev. 34, 925–951. https://doi.org/10.1111/j.1574-6976.2010.00217.x
Xu, T., Su, C., Hu, D., Li, F., Lu, Q., Zhang, T., Xu, Q., 2016. Molecular distribution and toxicity assessment of praseodymium by Spirodela polyrrhiza. J. Hazard. Mater. 312, 132–140.
Yufeng, Z., Lifen, Y., Kaoshan, C., Liang, D., 2007. Effects of neodymium on growth, pectinase activity and mycelium permeability of Fusarium oxysporum. J. Rare Earths 100–105.

Appendix A. Supplementary material

Table S1: ICP-AES and ICP-MS validity data. The data include the percentages of recovery of the oriental basma tobacco leaves certified material (INCT-OBTL-5, LGC Promochem, Molsheim, France), the limit of detection (LOD) and limit of quantification (LOQ).

Table S2: Summarized RNA-seq results of yeast exposed to La or Yb for 1 h. Each condition was compared to the non-REE-exposed control condition. Data are the log2FC expression. The left table presents differentially expressed genes with a padj < 0.01, while the right table includes the fold change values regardless of the padj value.

Table S3: Summarized proteomics results of yeast exposed to La or Yb at their respective EC_{50} for 1 h or 4 h. The left table presents differentially abundant proteins with a padj < 0.05, while the right table includes the fold change values regardless of the padj value.

Table S4: GO terms significantly represented in the set of differentially abundant (DA) proteins under La vs Ctrl exposure after 1 h. The tables are separated into biological process (BP), cellular component (CC) and molecular function (MF). Significantly enriched GO terms are identified in the DA downregulated proteins (blue), DA upregulated proteins (orange), or all DA proteins (grey).

Table S5: GO terms significantly enriched in the set of differentially abundant (DA) proteins under Yb vs Ctrl exposure after 1 h. The tables are separated into biological process (BP), cellular component (CC) and molecular function (MF). The significantly enriched GO terms are identified in the DA downregulated proteins (blue), DA upregulated proteins (orange) or all DA proteins (grey).

Table S6: GO terms significantly enriched in the set of differentially abundant (DA) proteins under Yb vs La exposure after 1 h. The tables are separated into biological process (BP), cellular component (CC) and molecular function (MF). The significantly enriched GO terms are identified in the DA downregulated proteins (blue), DA upregulated proteins (orange) or all DA proteins (grey).

Table S7: GO terms significantly enriched in the set of differentially expressed (DE) genes under Yb vs Ctrl exposure after 1 h. The tables are separated into biological process (BP),

cellular component (CC) and molecular function (MF). The significantly enriched GO terms are identified in the DE downregulated genes (blue), DE upregulated genes (orange) or all DE genes (grey).

Table S8: Summarized RNA-seq and proteomics results. Each condition was compared to the non-REE-exposed control condition. Cells were exposed to La or Yb at their respective EC_{50} for 1 h or 4 h, as indicated. The left table presents differentially expressed genes with a padj < 0.05 (PRO) and < 0.01 (RNA), while the right table includes the fold change values regardless of the padj value.

Table S9: GO terms significantly enriched in the set of differentially abundant (DA) proteins under La vs Ctrl exposure after 4 h. The tables are separated into biological process (BP), cellular component (CC) and molecular function (MF). The significantly enriched GO terms are identified in the DA downregulated proteins (blue), DA upregulated proteins (orange) or all DA proteins (grey).

Table S10: GO terms significantly enriched in the set of differentially abundant (DA) proteins under Yb vs Ctrl exposure after 4 h. The tables are separated into biological process (BP), cellular component (CC) and molecular function (MF). The significantly enriched GO terms are identified in the DA downregulated proteins (blue), DA upregulated proteins (orange) or all DA proteins (grey).

Table S11: GO terms significantly enriched in the set of differentially abundant (DA) proteins under Yb vs La exposure after 4 h. The tables are separated into biological process (BP), cellular component (CC) and molecular function (MF). The significantly enriched GO terms are identified in the DA downregulated proteins (blue), DA upregulated proteins (orange) or all DA proteins (grey).

Table S12: GO terms significantly enriched in the set of differentially expressed (DE) genes under La vs Ctrl exposure after 1 h. The tables are separated into biological process (BP), cellular component (CC) and molecular function (MF). The significantly enriched GO terms are identified in the DE downregulated genes (blue), DE upregulated genes (orange) or all DE genes (grey).

Table S13: GO terms significantly enriched in the set of differentially expressed (DE) genes under La vs Yb exposure after 1 h. The tables are separated into biological process (BP), cellular component (CC) and molecular function (MF). The significantly enriched GO terms are identified in the DE downregulated genes (blue), DE upregulated genes (orange) or all DE genes (grey).